

Stabilizing Off-Policy Training for Long-Horizon LLM Agent via Turn-Level Importance Sampling and Clipping-Triggered Normalization

Chenliang Li^{1*}, Adel Elmahdy², Alex Boyd², Zhongruo Wang³, Siliang Zeng⁴,
Alfredo Garcia¹, Parminder Bhatia², Taha Kass-Hout², Cao Xiao², Mingyi Hong⁴

¹Texas A&M University ²GE HealthCare
³Independent Researcher ⁴University of Minnesota

February 26, 2026

Abstract

Reinforcement learning (RL) algorithms such as PPO and GRPO are widely used to train large language models (LLMs) for multi-turn agentic tasks. However, in off-policy training pipelines, these methods often exhibit unstable optimization dynamics and are prone to performance collapse. Through empirical analysis, we identify two fundamental sources of instability in this setting: (1) a granularity mismatch between token-level policy optimization and turn-structured interactions, and (2) high-variance and unreliable gradient updates induced by off-policy importance sampling and inaccurate advantage estimation. To address these challenges, we propose SORL, Stabilizing Off-Policy Reinforcement Learning for Long-Horizon Agent Training. SORL introduces principled mechanisms that align policy optimization with the structure of multi-turn interactions and adaptively suppress unreliable off-policy updates, yielding more conservative and robust learning dynamics. Within this framework, we instantiate two stabilized algorithms: SO-PPO and SO-GRPO. Both algorithms are designed to mitigate gradient variance and prevent optimization collapse without requiring careful early stopping or heuristic tuning. We evaluate SO-PPO and SO-GRPO on a range of multi-turn search benchmarks, including general question answering, multi-hop question answering, and medical multiple-choice QA tasks. Experimental results show that both methods consistently prevent training instabilities and performance collapses observed in standard PPO and GRPO, maintain lower clipping ratios and more stable optimization trajectories, and achieve superior or comparable task performance. These results demonstrate that the proposed algorithm provides a practical, scalable, and general framework for stabilizing reinforcement learning in multi-turn LLM agent training.

1 Introduction

Reinforcement learning has significantly advanced the reasoning capabilities of large language models, enabling strong performance in domains such as mathematical problem solving (Jaech et al., 2024;

*This work was done during an internship at GE HealthCare, Bellevue, WA.

Corresponding authors: Chenliang Li (chenliangli@tamu.edu), and Adel Elmahdy (adel.elmahdy@gehealthcare.com).

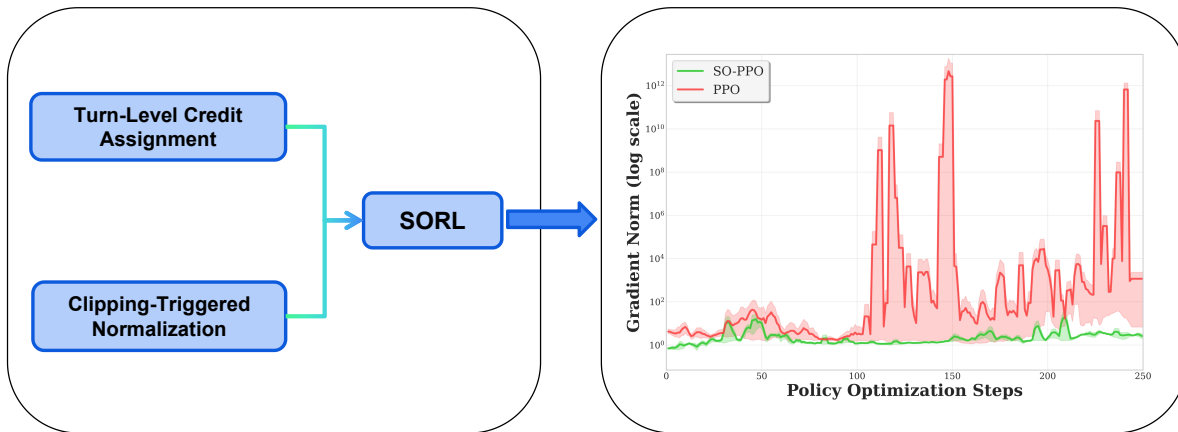


Figure 1: Illustration of the proposed SORL framework. The left panel shows the two key components of SORL, turn-level credit assignment and clipping-triggered normalization. The right panel reports policy gradient norms during training, demonstrating that the proposed algorithm effectively suppresses extreme gradient spikes and leads to more stable optimization dynamics.

Liu et al., 2024; Yu et al., 2025) and code generation (El-Kishky et al., 2025; Cui et al., 2025). Beyond these applications, RL has also shown promise in more agentic settings such as tool learning (Qian et al., 2025; Feng et al., 2025), where models learn to invoke external tools (e.g., web search engines), execute actions, and interact with real-world environments. Recent systems such as Deepseek V3 (Liu et al., 2024) and Kimi V2 (Team et al., 2025) have achieved state-of-the-art performance on both mathematical reasoning (e.g., AIME, Math-500) and agentic benchmarks (Jimenez et al., 2023). Despite these successes, the computational demands of multi-turn RL training pose significant practical challenges. These gains rely on numerous interaction samples, which are costly due to the large number of rollouts and multi-turn tool calls required during training. In practice, hardware and memory limits force each batch of collected samples to be split into several mini-batches (Schulman et al., 2017) and updated sequentially. This naturally induces a hybrid update mechanism where later updates become increasingly off-policy (Chen et al., 2023). To maximize sample efficiency under computational constraints, practitioners often adopt off-policy pipelines, and the resulting distribution mismatch is typically corrected using importance sampling (Nachum et al., 2017).

The shift to off-policy methods, while necessary for computational efficiency, introduces high variance and can destabilize training (Munos et al., 2016; Precup et al., 2000). To address this challenge, proximal policy optimization (PPO) (Schulman et al., 2017) constrains policy updates with a clipped surrogate objective. By limiting the impact of importance sampling ratios, PPO stabilizes learning even when mini-batch reuse makes later updates effectively off-policy. Building on this principle, recent studies (Zheng et al., 2025; Roux et al., 2025; Yan et al., 2025) refine importance sampling and clipping strategies to further enhance stability and efficiency.

Despite these advances, PPO training on multi-turn tasks still suffers from two core deficiencies: (1) token-level credit assignment misaligns with the natural granularity of multi-turn environments (Zeng et al., 2025), where reasoning unfolds through distinct turn-level stages (e.g., problem analysis, query formulation, information processing), and (2) off-policy updates increasingly dominate as training progresses, causing the data distribution to drift further from the current policy. This

growing off-policyness exacerbates the variance of importance sampling and undermines the reliability of advantage estimates, particularly for out-of-distribution tokens (Dorka et al., 2022). As a result, gradient variance increases over time, leading to unstable updates and potential policy collapse even under clipping.

To address these challenges, we propose **SORL**, a stabilizing off-policy reinforcement learning framework for long-horizon agent training, built on two key components.

First, **turn-level importance sampling** aligns policy optimization with the natural turn structure of multi-turn reasoning, enabling structure-aware credit assignment that balances the noise of token-level updates and the coarseness of sequence-level objectives. This design provides more precise attribution across different reasoning stages while mitigating variance amplification.

Second, **clipping-triggered normalization** stabilizes increasingly off-policy updates by explicitly correcting clipping-induced bias in PPO gradients. By retaining token-level clipping signals for variance control while leveraging turn-level importance ratios for credit assignment, SORL adaptively suppresses unreliable off-policy updates and yields more conservative and robust learning dynamics.

Our key contributions are as follows:

1. We empirically diagnose why vanilla PPO becomes unstable when applied to multi-turn LLM agent training under off-policy updates. Our analysis identifies two root causes unique to the agentic setting: (i) the granularity mismatch between token-level optimization and turn-level interactions, and (ii) the accumulation of variance from unreliable off-policy samples, where state-action pairs are poorly evaluated.
2. We propose a unified off-policy reinforcement learning framework that aligns policy optimization with the structure of multi-turn reasoning and stabilizes training under increasing off-policyness. Specifically, the framework integrates turn-level credit assignment with a clipping-triggered normalization mechanism to suppress unreliable updates, yielding more conservative gradient estimates and significantly improved training stability in long-horizon agent learning.
3. We demonstrate that the proposed framework is algorithm-agnostic and can be readily instantiated in other reinforcement learning methods beyond PPO, such as GRPO. Experimental results show that the resulting stabilized variant substantially improves training stability and prevents performance collapse compared to standard GRPO, highlighting the generality and practical effectiveness of our approach.

These contributions collectively establish **SORL** as a principled framework for stabilizing off-policy reinforcement learning in multi-turn LLM agent training, integrating theoretical insights with algorithmic design. By addressing both the granularity mismatch in credit assignment and the instability induced by increasingly off-policy updates, our approach enables more stable and conservative optimization. Empirically, SORL mitigates the training collapse observed in large-scale models and consistently improves task performance, offering a practical and scalable solution for reinforcement learning with multi-turn LLM agents.

2 Related Works

2.1 Reinforcement Learning with LLM Agents

Recent advances in reinforcement learning for large language models (LLMs) have primarily progressed along two main directions: (1) feedback-driven alignment and policy optimization, and (2) agentic tool use with long-horizon reasoning.

On the alignment side, RLHF (Ouyang et al., 2022) translates human or rule-based preferences into reward signals and optimizes policies using policy gradient methods, as exemplified by InstructGPT. Subsequent approaches such as direct preference optimization (DPO) (Rafailov et al., 2023) avoid explicit reward modeling, while other RL algorithms—including PPO (Schulman et al., 2017), GRPO (Shao et al., 2024), and RLOO (Ahmadian et al., 2024)—have been adapted to large models to balance stability and efficiency.

On the agentic side, methods such as ReAct (Yao et al., 2023), Give (He et al., 2024, 2025) integrate reasoning and acting through interleaved thought–action steps, while Reflexion (Shinn et al., 2023) leverages self-reflection and memory to enhance multi-turn decision making. Toolformer (Schick et al., 2023) demonstrates self-supervised learning of tool usage, and WebGPT (Nakano et al., 2021) introduces browser-based agents trained with human feedback. More recent systems, such as Search-R1 (Jin et al., 2025b), WebAgent-R1 (Wei et al., 2025), and WEBRL (Qi et al., 2024), extend this line of research to end-to-end reinforcement learning for web-based agents, where models are trained to perform retrieval, reasoning, and action within real-world interactive environments.

2.2 Off Policy Reinforcement Learning with LLM Agents

Off-policy reinforcement learning methods differ fundamentally from on-policy approaches by allowing the agent to learn from data generated by a policy different from the one currently being improved. This characteristic enables greater flexibility and data efficiency, as off-policy algorithms can reuse past experiences or observations collected under different policies. This property is particularly important in scenarios where data collection is costly or limited.

Recent work has extended these ideas to policy gradient methods tailored for off-policy learning in complex environments. The tapered off-policy REINFORCE (TOPR) algorithm (Roux et al., 2025) builds on the classic REINFORCE method (Williams, 1992) by introducing a tapered importance sampling scheme for the policy gradient. This tapering reduces the variance and instability that commonly arise in naive off-policy gradient methods, as it asymmetrically adjusts the importance weights to better balance learning from positive and negative examples. However, because TOPR relies heavily on trajectory-level rewards, it is not well-suited for scenarios that require more fine-grained credit assignment.

Another research line explores off-policy extensions of GRPO. ARPO (Lu et al., 2025) incorporates a replay buffer into GRPO’s sampling process, mixing on-policy and replayed samples to alleviate the zero-advantage issue, while RePO (Li et al., 2025a) reuses past outputs as off-policy samples with tailored replay strategies (e.g., recency-based, reward-oriented) to improve data efficiency and stability. Although these methods enhance sample utilization, they still require substantial training time, and their trajectory-level credit assignment often leads to slower convergence on multi-turn tasks.

2.3 Reinforcement Learning in Multi-turn Tasks

Recent advances in LLMs have increasingly leveraged reinforcement learning to enhance multi-turn reasoning and tool use capabilities (Chen et al., 2025; Cheng et al., 2025; Li et al., 2025c). The work on turn-level credit assignment by Zeng et al. (2025) introduces a novel RL framework that models multi-turn interactive tasks as Markov decision processes, enabling fine-grained credit allocation to individual reasoning and tool-use steps within a trajectory. Complementing this, the Search-R1 framework proposed by Jin et al. (2025a,b) similarly harnesses RL to train LLMs to reason

about when and how to use external search engines interactively. By framing the reasoning and search process as an end-to-end decision-making problem, Search-R1 encourages LLMs to generate informative queries and iteratively refine answers based on real-time feedback from the search tool. This work emphasizes the importance of multi-turn interactions to bridge the gap between internal textual reasoning and external information retrieval, demonstrating improved reasoning robustness and answer quality over traditional single-turn or passive retrieval approaches. Despite these advances, there remains a lack of algorithms specifically tailored to stabilize PPO in multi-turn LLM off-policy training. Our work addresses this gap by introducing a customized PPO variant that explicitly leverages turn-level structure, leading to more stable and scalable training.

3 Preliminaries

Notation. An autoregressive language model parameterized by θ is defined as a policy π_θ . We use x to denote a query and \mathcal{D} as the query set. Given a response y to a query x , its likelihood under the policy π_θ is denoted as $\pi_\theta(y | x) = \prod_{t=1}^{|y|} \pi_\theta(y_t | x, y_{<t})$, where $|y|$ denotes the number of tokens in y . A query-response pair (x, y) can be scored by a verifier r , resulting in a reward $r(x, y) \in [0, 1]$.

Turn-level MDP. We model multi-turn interactions as a Markov decision process $\mathcal{M} = (\mathcal{S}, \mathcal{A}, \mathcal{P}, \mathcal{R}, \gamma)$ defined at the granularity of turns. A turn is denoted by $y^k := (y_{t_k^{\text{start}}}, \dots, y_{t_k^{\text{end}}})$, and a full trajectory can be written as $y := (y^1; \dots; y^n)$ for n turns, where ‘;’ denotes token concatenation. Each state $s_k \in \mathcal{S}$ corresponds to the dialogue context at the beginning of turn k , which we define as $s_k := (x, y^1, y^2, \dots, y^{k-1})$. The transition $\mathcal{P}(s_{k+1} | s_k, a_k)$ updates the context with environment feedback (e.g., results from a tool call), and the reward $\mathcal{R}(s_k, a_k)$ evaluates the quality of the turn. The discount factor $\gamma \in (0, 1]$ balances present and future rewards. Unlike token-level MDPs, the unit of interaction here is the *turn*, with boundaries $[t_k^{\text{start}}, t_k^{\text{end}}]$, aligning credit assignment with the natural structure of reasoning and retrieval phases.

Proximal Policy Optimization (PPO). Using samples generated from the old policy $\pi_{\theta_{\text{old}}}$, PPO constrains the policy update within a proximal region of the old policy through the clipping mechanism. This allows for multiple gradient updates to the policy using the same batch of samples. Specifically, PPO employs the following objective for policy optimization:

$$\mathcal{J}_{\text{PPO}}(\theta) = \mathbb{E}_{x \sim \mathcal{D}, y \sim \pi_{\theta_{\text{old}}}(\cdot | x)} \left[\frac{1}{|y|} \sum_{t=1}^{|y|} \min \left(w_t(\theta) \hat{A}_t, \text{clip} \left(w_t(\theta), 1 - \epsilon, 1 + \epsilon \right) \hat{A}_t \right) \right], \quad (1)$$

where the importance ratio of the token y_t is defined as

$$w_t(\theta) = \frac{\pi_\theta(y_t | x, y_{<t})}{\pi_{\theta_{\text{old}}}(y_t | x, y_{<t})}, \quad (2)$$

where \hat{A}_t denotes the token-level advantage estimated by GAE based on the critic model \hat{V} . As discussed in related work, PPO has been widely used in many agentic tasks and performs well in single-turn settings. However, its performance in multi-turn settings is often unstable and prone to collapse; for example, Yuan et al. (2025) shows that PPO can fail in long reasoning tasks. In multi-turn settings, reward signals are typically provided only at the end of a long interaction. This delayed feedback leaves value predictions at intermediate states poorly constrained, and the resulting errors propagate backward through temporal-difference updates, compounding over many steps

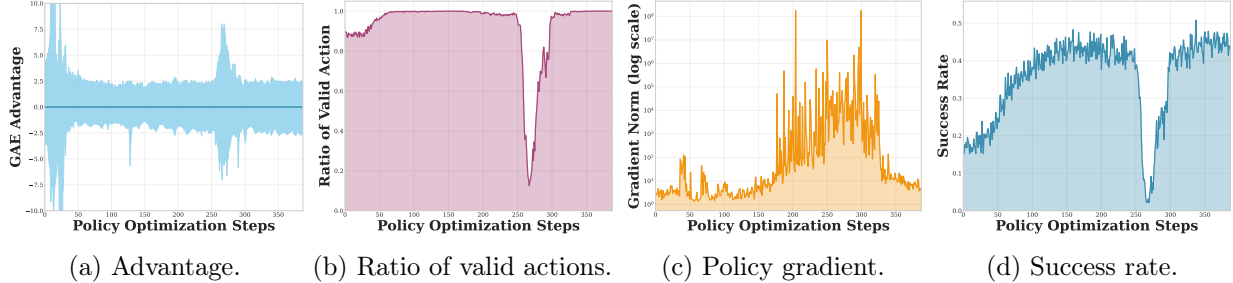


Figure 2: Observations from a failed training run using the Qwen2.5-7B base model with token-level PPO. From left to right, we report the estimated advantage (batch mean and variance), the ratio of valid actions (i.e., successful tool invocations), the ℓ_2 norm of the policy gradient, and the search-task success rate. All metrics are logged per training batch.

(Arjona-Medina et al., 2019). Another possible reason for PPO collapse is the high variance of importance sampling induced by the clipping mechanism in PPO. In long-horizon and off-policy settings, the importance ratios can become highly variable due to aggressive updates and factors such as training–inference mismatch, which may lead to unstable updates even with clipping. Similar clipping mechanisms are also used in other RL methods, such as GRPO. In our observations, once the variance of importance sampling becomes large, training is highly destabilized.

Verification. We provide both metric diagnostics and a representative failure case by examining a failed run of Qwen2.5-7B under token-level PPO (Fig. 2) in multi-turn search tasks. Specifically, we record the numerical metrics during training, and the results reveal two critical issues: (1) around steps 250–300, the critic assigns highly variable advantages while the ratio of valid actions sharply collapses, which is a typical signature of reward hacking; and (2) these unreliable samples subsequently trigger an explosion in the policy gradient norm, rapidly degrading performance and leading to a collapse in task success rate. This evidence confirms that critic estimation errors and variance accumulation can destabilize off-policy updates in multi-turn settings, thereby motivating the need for stabilization mechanisms beyond turn-level scaling. To further examine this behavior, we provide textual demonstrations in Appendix A.1, which show that prior to the collapse (at the 243rd and 247th epochs), importance sampling on format-related tokens exhibits high variance. Although these tokens are not critical to the LLM’s reasoning ability, such variance can accumulate and lead to a format collapse; after epoch 250, the LLM increasingly fails to follow the predefined output format, consistent with the behavior illustrated in Fig. 2(b).

4 Proposed Algorithm

In this section, we present our approach for stabilizing reinforcement learning in multi-turn LLM training, termed SORL (Stabilizing Off-Policy Reinforcement Learning for Long-Horizon Agent Training). Before diving into the details, we first introduce two key components of our algorithm and analyze how they stabilize training from the perspective of gradient norms.

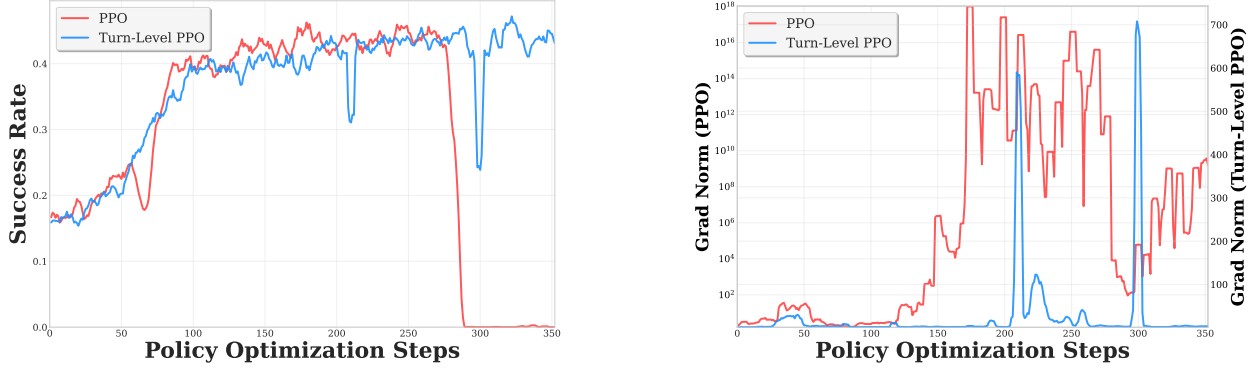


Figure 3: Comparison of token- and turn-level PPO on Qwen2.5-7B for the search task (single run for sanity check). **Left:** Success rates on the search task. **Right:** The ℓ_2 norm of the policy gradients.

4.1 Turn-Level Importance Sampling

In the previous section, we provided a representative failure case from a failed training run (see Appendix A.1), showing that token-level credit assignment in PPO can destabilize training and impair tool-calling stability. Building on this, we introduce the first component of our framework, which provides a simple and effective way to adjust the granularity of credit assignment. Specifically, for K total turns, with $[t_k^{\text{start}}, t_k^{\text{end}}]$ denoting the token positional boundaries of turn $k \in \{1, \dots, K\}$, we formulate a turn-level PPO objective:

$$\mathcal{J}_{\text{Turn-PPO}}(\theta) = \mathbb{E}_{x \sim \mathcal{D}, y \sim \pi_{\theta_{\text{old}}}(\cdot | x)} \left[\frac{1}{|y|} \sum_{k=1}^K \sum_{t=t_k^{\text{start}}}^{t_k^{\text{end}}} \min \left\{ w_k^{\text{turn}}(\theta) \hat{A}_t, \text{clip}(w_k^{\text{turn}}(\theta), 1 - \epsilon, 1 + \epsilon) \hat{A}_t \right\} \right], \quad (3)$$

where w_k^{turn} is a turn-level importance sampling weight. Inspired by the sequence-level weight used by Zheng et al. (2025), we define a turn-level variant as:

$$w_k^{\text{turn}}(\theta) := \left(\frac{\pi_{\theta}(y^k | x, y^{<k})}{\pi_{\theta_{\text{old}}}(y^k | x, y^{<k})} \right)^{\frac{1}{|y^k|}} \exp \left(\frac{1}{|y^k|} \sum_{t=t_k^{\text{start}}}^{t_k^{\text{end}}} \log \frac{\pi_{\theta}(y_t | x, y_{<t})}{\pi_{\theta_{\text{old}}}(y_t | x, y_{<t})} \right), \quad (4)$$

where the ratio is scaled by the length of the k^{th} turn, $|y^k|$, to stabilize the objective across turns of varying lengths. Next, we introduce a lemma showing that turn-level importance sampling induces a turn-wise aggregation of token-level advantages, such that all tokens within the same turn share a common, length-normalized credit signal. As a result, policy gradients are computed at the granularity of turns rather than individual tokens, aligning credit assignment with turn-level (action-level) interactions. To facilitate this analysis, we define the events under which clipping is inactive for the objective in Eq. 3:

$$\mathcal{B}_{\text{turn}}^+ := \{(k, t) : \hat{A}_t \geq 0, w_k^{\text{turn}}(\theta) \leq 1 + \epsilon\}, \quad \mathcal{B}_{\text{turn}}^- := \{(k, t) : \hat{A}_t < 0, w_k^{\text{turn}}(\theta) \geq 1 - \epsilon\}. \quad (5)$$

Let $\mathcal{B}_{\text{turn}} := \mathcal{B}_{\text{turn}}^+ \cup \mathcal{B}_{\text{turn}}^-$. When $\mathcal{B}_{\text{turn}}$ holds, the PPO objective reduces to the unclipped form $w_t \hat{A}_t$. In contrast, when $\mathcal{B}_{\text{turn}}^c$ occurs (clipping is active), it indicates a mismatch between the reference and current policies, and gradients of the corresponding tokens are set to zero.

Lemma 4.1. *The gradient of the objective function in Eq. 3 is given by*

$$\nabla_{\theta} \mathcal{J}_{\text{Turn-PPO}}(\theta) = \mathbb{E} \left[\frac{1}{|y|} \sum_{k=1}^K \underbrace{w_k^{\text{turn}}(\theta) \frac{\hat{A}^k}{|y^k|}}_{\text{Turn-Level Credit}} \nabla_{\theta} \log \pi_{\theta}(y^k | x, y^{<k}) \right], \quad (6)$$

where $|y^k| = t_k^{\text{end}} - t_k^{\text{start}} + 1$ and $\hat{A}^k := \sum_{t=t_k^{\text{start}}}^{t_k^{\text{end}}} \mathbb{1}_{\{(k,t) \in \mathcal{B}_{\text{turn}}\}} \hat{A}_t$.

Proof. We refer to Appendix A.2 for the proof. □

Lemma 4.1 highlights the effect of turn-level importance sampling. As shown in Eq. 6, all tokens within a turn share the same aggregated advantage \hat{A}^k , while advantages and clipping are still computed token-wise.

This implies that the policy gradient assigns credit at the granularity of turns rather than individual tokens, specifically due to the use of a shared turn-level importance weight. As a result, tokens within the same turn collectively reinforce or suppress the corresponding turn-level action, instead of competing for credit at the token level. Importantly, this modification does not alter how advantages are estimated or how clipping is applied. Instead, it reshapes how token-level signals are aggregated in the gradient, mitigating large gradient norms induced by token-level fluctuations while preserving fine-grained advantage estimation.

This turn-level structure arises from using a shared geometric-mean importance ratio within each turn and aggregating unclipped token-level contributions in $\mathcal{B}_{\text{turn}}$. This is consistent with our experiments and prior work (Zhou et al., 2024; Zeng et al., 2025).

Validation. We compare token-level PPO in Eq. 1 and turn-level PPO in Eq. 3 on the search task using the Qwen2.5-7B base model. As shown in Fig. 3, turn-level importance sampling substantially reduces the norm of the PPO policy gradient, bringing it from a logarithmic scale to a normal scale. This reduction effectively prevents the catastrophic gradient explosion observed in standard token-level PPO and leads to more stable optimization dynamics during training. Meanwhile, we observe that the performance curve of turn-level PPO still exhibits occasional sharp drops. These drops coincide with spikes in the gradient norm (approximately 1000–2000), indicating that instability can still arise even under turn-level importance sampling. As a result, turn-level PPO fails to consistently reach its best performance.

4.2 Clipping-Triggered Normalization

While turn-level importance sampling alleviates gradient explosion by aligning credit assignment with the turn structure, the remaining instability suggests that granularity mismatch alone does not fully explain the observed optimization failures. In highly off-policy regimes, the reliability of sampled data itself becomes a critical factor affecting training stability, independent of how credit is assigned. To better understand this effect, we begin with a general analysis of off-policy PPO updates by examining the gradient decomposition. This analysis motivates a normalization mechanism that targets unreliable off-policy updates and can be naturally integrated into clipping-based reinforcement learning algorithms. In the following, we apply this mechanism to the turn-level PPO developed in Section 4.1, yielding a more robust and stable optimization procedure.

In this section, we investigate the growth of the policy gradient norm during training by examining the distribution of importance sampling ratios at the mid-training stage. As shown in the left panel of Fig. 4, the distribution is heavy-tailed, with some samples exhibiting extremely large or small

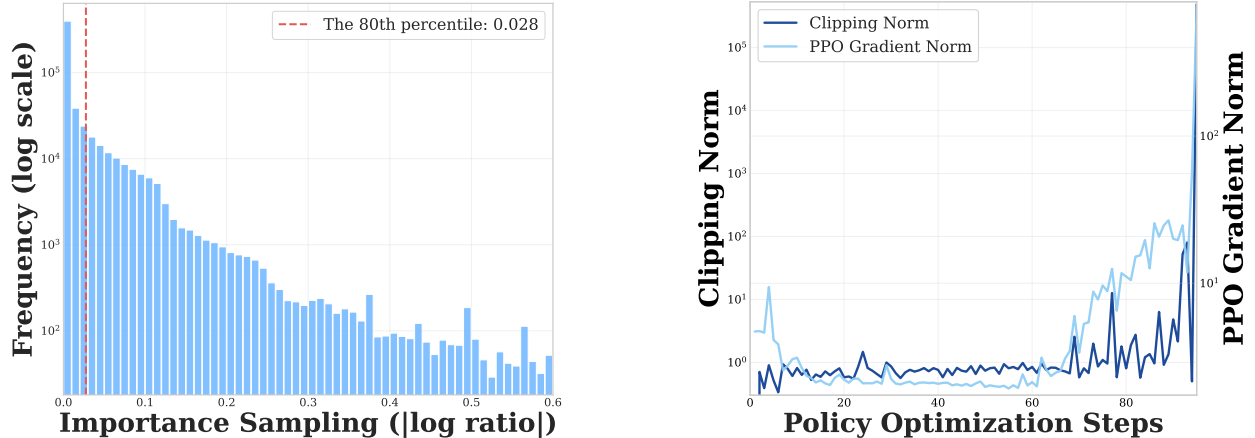


Figure 4: Additional diagnostic metrics for token-level PPO on Qwen2.5-7B. **Left:** Distribution of importance sampling ratios, shown as the absolute value of the log ratio across training. The pronounced heavy-tailed behavior indicates substantial variance in importance weights. **Right:** Evolution of the L2 norm of the clipping bias term alongside the PPO gradient norm over policy optimization steps. Both quantities exhibit rapid growth during training, highlighting increasing instability in the optimization dynamics.

importance sampling ratios, a phenomenon that typically arises when the training batch becomes highly off-policy. To mitigate this effect and avoid updates dominated by batches with high-variance importance sampling ratios, we introduce the second component of our algorithm, termed Clipping-Triggered Normalization. To motivate this design, we analyze the gradient of the PPO objective by decomposing it according to whether clipping is active. To introduce what clipping bias is, we begin by defining the events under which clipping is inactive:

$$\begin{aligned} \mathcal{B}^+ &:= \{t : \hat{A}_t \geq 0, w_t(\theta) \leq 1 + \epsilon\}, \\ \mathcal{B}^- &:= \{t : \hat{A}_t < 0, w_t(\theta) \geq 1 - \epsilon\}. \end{aligned}$$

These sets correspond to token positions where the PPO surrogate objective reduces to the unclipped importance weighted objective. We define $\mathcal{B} := \mathcal{B}^+ \cup \mathcal{B}^-$. The complement set \mathcal{B}^c consists of all remaining token positions where clipping is active. Then we can formally decompose the PPO gradient as follows:

Lemma 4.2. *The PPO gradient can be decomposed as*

$$\frac{\partial \mathcal{J}_{\text{PPO}}(\theta)}{\partial \log \pi_\theta} = \underbrace{\mathbb{E} \left[\frac{1}{|y|} \sum_{t=1}^{|y|} w_t \nabla_\theta \log \pi_\theta \hat{A}_t \right]}_{\text{Policy Gradient}} - \underbrace{\mathbb{E} \left[\frac{1}{|y|} \sum_{t=1}^{|y|} \mathbb{1}_{t \in \mathcal{B}^c} w_t \hat{A}_t \right]}_{C(\theta): \text{Clipping Bias}}, \quad (7)$$

where \hat{A}_t denotes the advantage estimate by the critic using the GAE method.

Proof. We refer to Appendix A.3 for the proof of Lemma 4.2. □

Algorithm 1: *SO-PPO*

Input: Initialize policy π_0 , step size η , dataset \mathcal{D} , and maximum generation length L .
for iteration $k = 0, 1, \dots, K - 1$ **do**
 Data Sampling I: Sample a batch of queries $x \sim \mathcal{D}$ and generate agent trajectories $\tau := y_{0:L} \sim \pi_k$.
 Data Sampling II: For each trajectory, split it into turn-level state-action pairs $(s_0, a_0), (s_1, a_1), \dots$ (e.g., using a loss mask or $\langle \text{eot} \rangle$ tokens).
 Gradient Estimation: Compute the gradient as in Eq. 3.
 Clipping-Triggered Normalization: Compute the clipping bias norm and form the surrogate gradient in Eq. 12 with sampled agent trajectories τ .
 Policy Improvement: Update the policy using the surrogate gradient.
 Policy Evaluation: Update the critic using the TD error.
end for

From the gradient decomposition in Lemma 4.2, the PPO gradient can be expressed as the sum of a standard policy gradient term and a clipping bias term $C(\theta)$. The former corresponds to the vanilla off-policy policy gradient without clipping, where all tokens contribute uniformly to the update, while the latter arises from the indicator $\mathbb{1}_{t \in \mathcal{B}^c}$ and captures the contribution of tokens for which clipping is active. The clipping mechanism stabilizes optimization by suppressing excessively large updates, and the resulting clipping bias term selectively removes gradient contributions from clipped tokens, introducing bias into the gradient estimate.

Validation. We study how the clipping bias evolves during training and how it relates to the PPO gradient by running token-level PPO on the Qwen2.5-7B base model. Specifically, we track the L2 norms of the clipping bias term $C(\theta)$ and the PPO gradient $\nabla \mathcal{J}_{\text{PPO}}$ over optimization steps (right panel of Fig. 4). We find that the clipping bias and the PPO gradient norm are clearly correlated and tend to increase together as training proceeds. Moreover, the clipping bias shows larger fluctuations in later stages of training. A large clipping bias means that many clipped tokens in the current batch contribute gradients with large norms, which indicates that this batch is strongly off-policy. As a result, the policy updates become less stable in later training, when off-policy effects are more pronounced.

Motivated by this observation, we incorporate a new stabilization principle into the turn-level PPO formulation (Section 4.1). Specifically, we propose a surrogate gradient estimator that reweights each sampled generation according to its clipping bias, thereby adaptively downweighting highly off-policy updates and suppressing destabilizing gradients. From a scaling perspective, turn-level importance sampling treats each turn as a single optimization unit, weighting it by the turn-level importance ratio and the cumulative unclipped advantage, normalized by turn length. This results in a surrogate objective for turn-level PPO with an explicit clipping-bias correction, characterized by the following clipping bias term:

$$C_{\text{turn}}(\theta) := \mathbb{E}_{\tau \sim \pi_{\theta}} \left[\frac{1}{|y|} \sum_{t=1}^{|y|} \mathbb{1}_{t \in \mathcal{B}_{\text{turn}}^c} w_t^{\text{turn}}(\theta) \hat{A}_t \right]. \quad (8)$$

Intuitively, the norm of the clipping bias reflects the degree to which a batch is affected by off-policy samples: a larger clipping bias indicates that a substantial fraction of updates are dominated by clipped, and hence unreliable, importance ratios. Rescaling the policy update by the inverse of this norm therefore adaptively reduces the effective step size when off-policy variance dominates.

Based on this idea, we define the stabilized policy gradient as

$$\nabla_{\theta} \mathcal{J}_{\text{SO-PPO}}(\theta) := \frac{1}{\|C_{\text{turn}}(\theta)\|_2} \nabla_{\theta} \mathcal{J}_{\text{Turn-PPO}}(\theta). \quad (9)$$

In expectation, both the turn-level PPO gradient and the clipping bias are defined over trajectories sampled from the same policy:

$$\nabla_{\theta} \mathcal{J}_{\text{Turn-PPO}}(\theta) := \mathbb{E}_{\tau \sim \pi_{\theta}} [\nabla_{\theta} \mathcal{J}_{\text{Turn-PPO}}(\theta; \tau)], \quad (10)$$

$$C_{\text{turn}}(\theta) := \mathbb{E}_{\tau \sim \pi_{\theta}} [C_{\text{turn}}(\theta; \tau)]. \quad (11)$$

In practice, these expectations are approximated using the same mini-batch of sampled trajectories, yielding the following Monte Carlo estimator:

$$\nabla_{\theta} \hat{\mathcal{J}}_{\text{SO-PPO}}(\theta) := \frac{1}{\max(\|\hat{C}_{\text{turn}}(\theta)\|_2, \delta)} \nabla_{\theta} \hat{\mathcal{J}}_{\text{Turn-PPO}}(\theta), \quad (12)$$

where both $\hat{C}_{\text{turn}}(\theta)$ and $\nabla_{\theta} \hat{\mathcal{J}}_{\text{Turn-PPO}}(\theta)$ are computed from the same set of trajectories $\{\tau^{(i)}\}_{i=1}^B$ sampled from the current policy $\tau^{(i)} \sim \pi_{\theta}$. The constant $\delta > 0$ enforces a lower bound on the normalization factor, preventing excessively large updates when the estimated clipping bias is small and we set $\delta = 1$ in all experiments.

Fig. 1 illustrates the two components of our proposed algorithm SO-PPO and shows how it effectively reduces the norm of the policy gradient. We then present SO-PPO in Algorithm 1.

4.3 Extension to GRPO

Although our analysis in Lemma 4.2 focuses on PPO, the core stabilization components are not specific to a particular algorithm and can be readily transferred to other reinforcement learning methods. In this subsection, we use GRPO as a representative example to demonstrate the generality of our framework.

Notably, the clipping-triggered normalization can be incorporated into the GRPO framework, yielding a stabilized variant that we refer to as SO-GRPO. Unlike standard PPO, GRPO performs credit assignment at the trajectory level via its group-level surrogate. We therefore forego turn-level importance sampling in this context. Formally, GRPO optimizes an objective of the form:

$$J_{\text{GRPO}}(\theta) = \mathbb{E} \left[\min \left(w(\theta) \hat{A}^{\text{grp}}, \text{clip}(w(\theta), 1 - \epsilon, 1 + \epsilon) \hat{A}^{\text{grp}} \right) \right], \quad (13)$$

Following GRPO (Shao et al., 2024), importance sampling is performed at the token level. For a trajectory $\tau = (y_1, \dots, y_{|y|})$ sampled from the old policy $\pi_{\theta_{\text{old}}}$, the token-level importance ratio is defined as

$$w_t(\theta) := \frac{\pi_{\theta}(y_t | x, y_{<t})}{\pi_{\theta_{\text{old}}}(y_t | x, y_{<t})}.$$

In the GRPO surrogate objective, this token-level ratio is combined with a group-level advantage that is shared across all tokens within the same trajectory. Specifically, given a group of G sampled responses $\{\tau_i\}_{i=1}^G$ with trajectory-level rewards $\{r_i\}_{i=1}^G$, the group advantage is defined as

$$\hat{A}^{\text{grp}}(\tau_i) := \frac{r_i - \text{mean}(\{r_j\}_{j=1}^G)}{\text{std}(\{r_j\}_{j=1}^G)},$$

Algorithm 2: SO-GRPO

Input: Initialize policy π_0 , step size η , dataset \mathcal{D} , group size G , and maximum generation length L .
for iteration $k = 0, 1, \dots, K - 1$ **do**
 Data Sampling I: Sample a batch of queries $x \sim \mathcal{D}$.
 Data Sampling II: For each query x , sample a group of G responses $\{\tau_i := y_{0:L}^{(i)}\}_{i=1}^G \sim \pi_k(\cdot|x)$.
 Reward & Advantage: Compute rewards $\{r(x, \tau_i)\}_{i=1}^G$ and form group advantages $\{\hat{A}^{\text{grp}}(\tau_i)\}_{i=1}^G$ (e.g., normalized within the group).
 Gradient Estimation: Compute the GRPO gradient as in Eq. 13 (token-level ratios with shared group advantage).
 Clipping-Triggered Normalization: Compute the clipping bias norm and form the surrogate gradient for SO-GRPO (Eq. 15) using the sampled groups $\{\tau_i\}_{i=1}^G$.
 Policy Improvement: Update the policy using the surrogate gradient.
end for

and is assigned uniformly to all tokens t in τ_i . To apply the proposed clipping-triggered normalization mechanism, we compute the clipping bias using these token-level importance ratios together with the shared group-level advantages.

$$C_{\text{GRPO}}(\theta) := \mathbb{E} \left[\frac{1}{|y|} \sum_{t=1}^{|y|} \mathbb{1}_{t \in \mathcal{B}^c} w_t(\theta) \hat{A}^{\text{grp}} \right]. \quad (14)$$

Here, \mathcal{B} is defined analogously to the clipping set in PPO, with \hat{A}^{grp} replacing the advantage, and \mathcal{B}^c denotes its complement, which measures the contribution of samples whose importance ratios fall outside the trust region. The stabilized GRPO update is then defined analogously to SO-PPO:

$$\nabla_{\theta} J_{\text{SO-GRPO}}(\theta) := \frac{1}{\|C_{\text{GRPO}}(\theta)\|_2} \nabla_{\theta} J_{\text{GRPO}}(\theta).$$

Similar to SO-PPO, both the GRPO gradient and its clipping bias admit Monte Carlo estimators based on the same set of sampled trajectories. Specifically, the GRPO gradient and clipping bias can be written in expectation as

$$\nabla_{\theta} J_{\text{GRPO}}(\theta) := \mathbb{E}_{\tau \sim \pi_{\theta}} [\nabla_{\theta} J_{\text{GRPO}}(\theta; \tau)], \quad C_{\text{GRPO}}(\theta) := \mathbb{E}_{\tau \sim \pi_{\theta}} [C_{\text{GRPO}}(\theta; \tau)].$$

In practice, both quantities are estimated using the same mini-batch of sampled trajectories, yielding the Monte Carlo estimator

$$\nabla_{\theta} \hat{J}_{\text{SO-GRPO}}(\theta) := \frac{1}{\max(\|\hat{C}_{\text{GRPO}}(\theta)\|_2, \delta)} \nabla_{\theta} \hat{J}_{\text{GRPO}}(\theta), \quad (15)$$

where $\hat{C}_{\text{GRPO}}(\theta)$ and $\nabla_{\theta} \hat{J}_{\text{GRPO}}(\theta)$ are computed from the same sampled groups. This ensures a consistent implementation of clipping-triggered normalization across algorithms.

This yields a lightweight yet effective variant: SO-GRPO rescales the Monte Carlo policy gradient by the inverse clipping-bias norm, thereby downweighting trajectory groups that exhibit extreme off-policy behavior. Since GRPO already performs credit assignment at the trajectory level via group advantages, we do not introduce additional turn-level importance sampling. The algorithm of SO-GRPO is summarized in Alg.2. Before concluding this section, we briefly discuss the advantages of the proposed algorithm.

Stability. The proposed framework stabilizes training by reducing the magnitudes of the policy gradients through two complementary mechanisms. Turn-level credit assignment mitigates variance amplification from misaligned token-level updates, while clipping-triggered normalization adaptively downweights highly off-policy batches via their clipping bias. Together, these components suppress extreme gradient spikes and yield more stable optimization dynamics.

Generality. The formulation is flexible enough to recover existing LLM training methods (e.g., GRPO) through specific choices of advantage design. This generality allows algorithms developed for advantage estimation to be directly applied as special cases within our framework.

5 Experiments

We conduct comprehensive numerical evaluations of our proposed SORL algorithm (Algorithm 1) and compare its performance against the state-of-the-art baseline, Search-R1 (Jin et al., 2025b). Our experimental results demonstrate two key advantages of the proposed approach: (1) the combination of turn-level importance sampling and clipping-bias correction significantly enhances training stability compared to standard PPO, preventing the performance collapses commonly observed in multi-turn agent training, and (2) SO-PPO and SO-GRPO maintain consistently lower clipping ratios throughout training, indicating more reliable gradient updates.

Experimental Setup. Following the experimental setup of Search-R1 (Jin et al., 2025b), we conduct our experiments using the Qwen-2.5-7B (Base) model (Bai et al., 2023) as the base policy. For retrieval, we employ the 2018 Wikipedia dump (Karpukhin et al., 2020) as our knowledge source and the E5 embeddings (Wang et al., 2022) as the retriever. To ensure fair comparison with existing methods, we follow Lin et al. (2023) and consistently retrieve three passages across all retrieval-based approaches. We evaluate SORL on two benchmark datasets: (1) Natural Questions (NQ) (Kwiatkowski et al., 2019) and (2) HotpotQA (Ho et al., 2020). These datasets present diverse multi-hop reasoning and search challenges that require effective coordination between information retrieval and reasoning steps, making them ideal testbeds for evaluating the stability and effectiveness of our turn-level optimization approach. For complete implementation details, refer to Appendix A.4.

Evaluation. For evaluation, we evaluate on the test sets of the NQ and HotpotQA datasets to assess model performance on each domain. Exact Match (EM) is used as the primary evaluation metric, which measures the percentage of predictions that exactly match the ground-truth answers after standard normalization. EM provides a strict assessment of whether our multi-turn approach successfully retrieves and synthesizes correct information through the search and reasoning process.

Training Stability and Performance. Fig. 5 compares the training dynamics of standard PPO and SO-PPO on the NQ and HotpotQA datasets. All methods exhibit rapid initial improvement, indicating that PPO can identify effective policies early in training. However, their long-term behaviors diverge substantially. Token-level PPO shows pronounced instability: after reaching peak performance, the policy undergoes sharp collapses, resulting in performance that is significantly worse than that of earlier checkpoints. This degradation is consistent with our analysis, which shows that highly off-policy training batches with large importance sampling ratios can destabilize gradient updates. As a result, careful early stopping is required to retain the best-performing checkpoint, complicating the training procedure. In contrast, SORL maintains steady performance improvements throughout the entire optimization horizon without experiencing such collapses.

Ablation Study. In Appendix A.5, we further evaluate our algorithm under different off-policy settings by fixing the total training batch size while decreasing the minibatch size, which

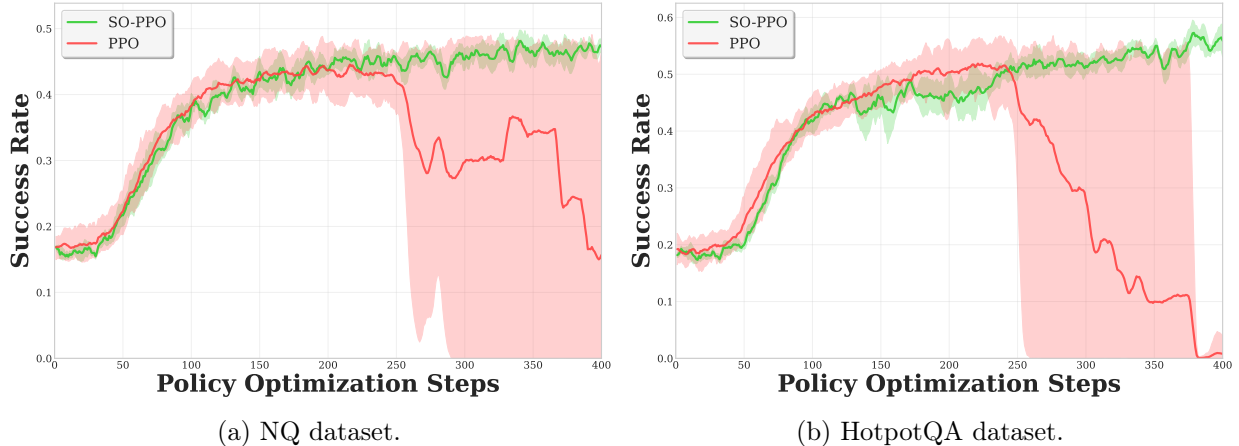


Figure 5: Experimental results of Qwen-2.5-7B policy models. Results are averaged over three trials. We report the average success rate on the NQ and HotpotQA datasets.

increases the degree of off-policyness during optimization. The results show that the proposed algorithm SORL remains stable under these more challenging conditions. Moreover, Figure 8 reports consistently smaller KL divergence throughout training. Together, these findings confirm that our method effectively reduces the magnitude of unstable updates and improves training stability.

This stability stems from two key mechanisms: (1) the turn-level importance sampling aligns credit assignment with the natural structure of reasoning-search interactions, reducing the granularity mismatch that contributes to instability, and (2) the clipping-triggered normalization adaptively scales gradient updates, reducing the influence of tokens with high variance importance sampling. As a result, SO-PPO achieve both competitive peak performance and robust convergence without requiring early stopping or careful checkpoint selection.

To further validate the effectiveness of our GRPO variant, we compare GRPO, GSPO (Zheng et al., 2025), and the proposed SO-GRPO on the NQ dataset. GSPO is a recently proposed stabilization method that replaces token-level importance ratios in GRPO with sequence-level likelihood ratios. As shown in Fig. 6, SO-GRPO achieves substantially improved training stability over GRPO and further outperforms GSPO. While GSPO already improves stability by adopting sequence-level importance sampling, our results show that clipping-triggered normalization provides additional and more consistent stabilization benefits in off-policy training.

We further evaluate the performance of SO-PPO and SO-GRPO on medical tasks to assess their generalization ability in a domain distinct from open-domain search. Specifically, we use the AlphaMed19K (Liu et al., 2025) dataset for training, with Wikipedia serving as the retrieval source. To ensure consistency across experiments and datasets, we adopt the prompt template shown in Appendix A.5 for all training runs. The hyperparameter configuration for the medical dataset follows the same settings used in the NQ and HotpotQA experiments.

Baselines. We compare our method against several 8B-scale baselines commonly used in agentic tasks: (1) **RAG**: Retrieval-augmented generation (Glass et al., 2022; Li et al., 2025b) using the tool-following instructions, where external documents are retrieved to supplement the model’s responses. Note that the Llama-3.1-8B-Instruct model is used without additional training in this setting. (2) **COT**: Chain-of-Thought prompting (Wei et al., 2022), which encourages the model to generate explicit reasoning steps before producing an answer. (3) **Search-R1**: Search-R1

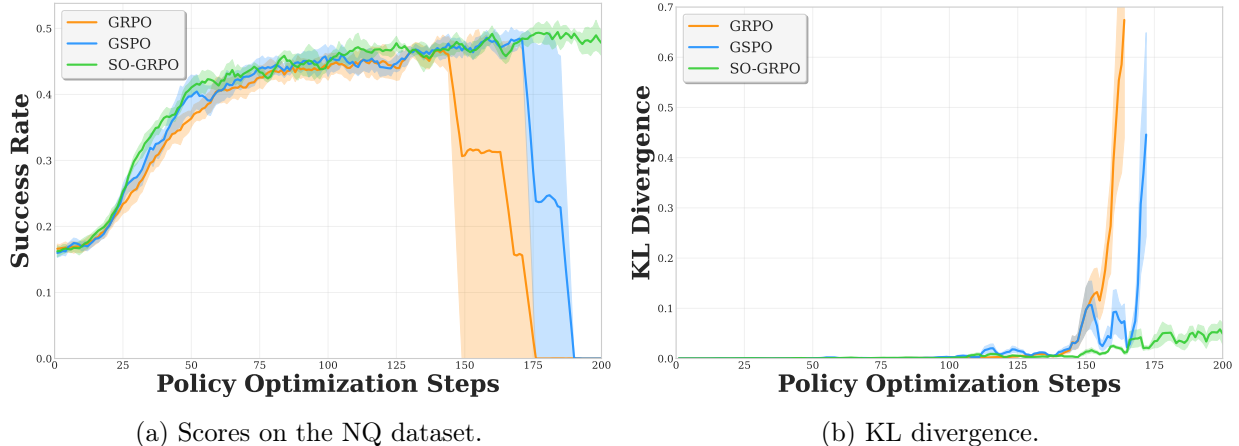


Figure 6: Comparison of GRPO, GSPO, and SO-GRPO on the NQ dataset. (a) Success rates show that GRPO and GSPO collapse during training, whereas SO-GRPO remains stable. (b) KL divergence exhibits large spikes for GRPO and GSPO, while SO-GRPO stays near zero.

framework (Jin et al., 2025b), where we train the model using PPO and evaluate using the checkpoint at the 150th optimization step (2 epochs). (4) **SORL**: Our proposed algorithm, evaluated using the checkpoint at the 150th step (2 epochs).

Evaluation Datasets. To comprehensively evaluate the algorithm’s performance on medical tasks, we consider both in-domain and out-of-domain benchmarks. For in-domain evaluation, we use MedQA (Jin et al., 2020) and MedMCQA (Pal et al., 2022). For out-of-domain evaluation, we include PubMedQA (Jin et al., 2019), the medical subset of MMLU (Wang et al., 2024), and MedXpert (Zuo et al., 2025). We exclude GPQA (Rein et al., 2024) as it does not contain a medically relevant subset.

Performance. Table 1 demonstrates that our training approach not only stabilizes multi-turn optimization but also enables models that initially lack tool-use capability to reliably perform retrieval and acquire domain knowledge. The poor performance of RAG highlights this limitation when retrieval is introduced without reinforcement learning. In contrast, both SO-PPO and SO-GRPO substantially improve performance across medical QA benchmarks. Specifically, SO-PPO achieves the best average accuracy among PPO-based retrieval-enhanced methods (53.88%), consistently outperforming the Search-R1 baseline on both in-domain and out-of-domain evaluations. Moreover, SO-GRPO further improves overall performance, attaining the highest average accuracy (55.34%) across all retrieval-augmented and RL-enhanced approaches. These results indicate that our framework not only stabilizes training but also translates improved optimization dynamics into stronger generalization and task performance.

6 Conclusion

We investigated the instability of off-policy reinforcement learning in multi-turn LLM agent training and identified two key causes: the mismatch between token-level optimization and turn-structured interactions, and the accumulation of high-variance updates under increasingly off-policy training. To address these issues, we proposed **SORL**, a framework that combines turn-level credit assignment

Table 1: Performance of 8B medical LLMs across in-domain[†] and out-of-domain* benchmarks (accuracy %). Bold numbers indicate the best performance, while underlined numbers indicate the second-best performance.

Model	In-Domain [†]		Out-of-Domain*			Avg.
	MedQA	MedMCQA	PubMedQA	MMLU-M	MedXpert	
<i>Inference-Based Methods (No Retrieval)</i>						
Llama-3.1-8B-Instruct (Direct Inference)	45.20	52.40	62.00	40.70	13.00	42.66
Llama-3.1-8B-Instruct (CoT)	48.62	59.80	64.40	54.20	13.02	48.01
MedLlama-3-8B (CoT)	66.60	53.40	64.40	45.70	11.04	48.23
<i>Retrieval-Augmented and RL-Enhanced Methods</i>						
Llama-3.1-8B-Instruct (RAG)	8.90	11.30	16.80	4.90	9.20	10.22
Llama-3.1-8B-Instruct (Search-R1)	53.40	54.00	60.20	49.50	9.77	45.37
Llama-3.1-8B-Instruct (SO-PPO, Ours)	<u>64.80</u>	<u>60.80</u>	<u>68.31</u>	<u>59.78</u>	<u>15.75</u>	<u>53.88</u>
Llama-3.1-8B-Instruct (SO-GRPO , Ours)	67.32	62.40	68.65	61.24	17.06	55.34

[†]In-domain benchmarks. *Out-of-domain benchmarks.

with clipping-triggered normalization to stabilize policy optimization. Instantiations of SORL with PPO and GRPO effectively suppress unreliable off-policy updates and yield more stable optimization dynamics. Experiments on multi-turn search and medical QA benchmarks demonstrate that SORL consistently improves training stability and robustness without requiring heuristic tuning or early stopping.

References

- Arash Ahmadian, Chris Cremer, Matthias Gallé, Marzieh Fadaee, Julia Kreutzer, Olivier Pietquin, Ahmet Üstün, and Sara Hooker. Back to basics: Revisiting reinforce style optimization for learning from human feedback in llms. *arXiv preprint arXiv:2402.14740*, 2024.
- Jose A Arjona-Medina, Michael Gillhofer, Michael Widrich, Thomas Unterthiner, Johannes Brandstetter, and Sepp Hochreiter. Rudder: Return decomposition for delayed rewards. *Advances in Neural Information Processing Systems*, 32, 2019.
- Jinze Bai, Shuai Bai, Yunfei Chu, Zeyu Cui, Kai Dang, Xiaodong Deng, Yang Fan, Wenbin Ge, Yu Han, Fei Huang, et al. Qwen technical report. *arXiv preprint arXiv:2309.16609*, 2023.
- Mingyang Chen, Tianpeng Li, Haoze Sun, Yijie Zhou, Chenzheng Zhu, Haofen Wang, Jeff Z Pan, Wen Zhang, Huajun Chen, Fan Yang, et al. Learning to reason with search for llms via reinforcement learning. *arXiv preprint arXiv:2503.19470*, 2025.
- Xing Chen, Dongcui Diao, Hechang Chen, Hengshuai Yao, Haiyin Piao, Zhixiao Sun, Zhiwei Yang, Randy Goebel, Bei Jiang, and Yi Chang. The sufficiency of off-policyness and soft clipping: PPO is still insufficient according to an off-policy measure. *Proceedings of the AAAI Conference on Artificial Intelligence*, 37(6):7078–7086, 2023.
- Jie Cheng, Ruixi Qiao, Lijun Li, Chao Guo, Junle Wang, Gang Xiong, Yisheng Lv, and Fei-Yue Wang. Stop summation: Min-form credit assignment is all process reward model needs for reasoning. *arXiv preprint arXiv:2504.15275*, 2025.
- Ganqu Cui, Lifan Yuan, Zefan Wang, Hanbin Wang, Wendi Li, Bingxiang He, Yuchen Fan, Tianyu Yu, Qixin Xu, Weize Chen, et al. Process reinforcement through implicit rewards. *arXiv preprint arXiv:2502.01456*, 2025.
- Nicolai Dorka, Tim Welschehold, Joschka Bödecker, and Wolfram Burgard. Adaptively calibrated critic estimates for deep reinforcement learning. *IEEE Robotics and Automation Letters*, 8(2): 624–631, 2022.
- Ahmed El-Kishky, Alexander Wei, Andre Saraiva, Borys Minaiev, Daniel Selsam, David Dohan, Francis Song, Hunter Lightman, Ignasi Clavera, Jakub Pachocki, et al. Competitive programming with large reasoning models. *arXiv preprint arXiv:2502.06807*, 2025.
- Jiazhan Feng, Shijue Huang, Xingwei Qu, Ge Zhang, Yujia Qin, Baoquan Zhong, Chengquan Jiang, Jinxin Chi, and Wanjun Zhong. Retool: Reinforcement learning for strategic tool use in llms. *arXiv preprint arXiv:2504.11536*, 2025.
- Michael Glass, Gaetano Rossiello, Md Faisal Mahbub Chowdhury, Ankita Naik, Pengshan Cai, and Alfio Gliozzo. Re2g: Retrieve, rerank, generate. In *Proceedings of the 2022 Conference of the North American Chapter of the Association for Computational Linguistics: Human Language Technologies*, pp. 2701–2715, 2022.
- Jiashu He, Mingyu Derek Ma, Jinxuan Fan, Dan Roth, Wei Wang, and Alejandro Ribeiro. Give: Structured reasoning of large language models with knowledge graph inspired veracity extrapolation. *arXiv preprint arXiv:2410.08475*, 2024.

- Jiashu He, Jinxuan Fan, Bowen Jiang, Ignacio Houine, Dan Roth, and Alejandro Ribeiro. Self-give: Associative thinking from limited structured knowledge for enhanced large language model reasoning. *arXiv preprint arXiv:2505.15062*, 2025.
- Xanh Ho, Anh-Khoa Duong Nguyen, Saku Sugawara, and Akiko Aizawa. Constructing a multi-hop qa dataset for comprehensive evaluation of reasoning steps. *arXiv preprint arXiv:2011.01060*, 2020.
- Aaron Jaech, Adam Kalai, Adam Lerer, Adam Richardson, Ahmed El-Kishky, Aiden Low, Alec Helyar, Aleksander Madry, Alex Beutel, Alex Carney, et al. Openai o1 system card. *arXiv preprint arXiv:2412.16720*, 2024.
- Carlos E Jimenez, John Yang, Alexander Wettig, Shunyu Yao, Kexin Pei, Ofir Press, and Karthik Narasimhan. Swe-bench: Can language models resolve real-world github issues? *arXiv preprint arXiv:2310.06770*, 2023.
- Bowen Jin, Jinsung Yoon, Priyanka Kargupta, Serkan O Arik, and Jiawei Han. An empirical study on reinforcement learning for reasoning-search interleaved llm agents. *arXiv preprint arXiv:2505.15117*, 2025a.
- Bowen Jin, Hansi Zeng, Zhenrui Yue, Jinsung Yoon, Serkan Arik, Dong Wang, Hamed Zamani, and Jiawei Han. Search-r1: Training LLMs to reason and leverage search engines with reinforcement learning. In *Second Conference on Language Modeling (COLM)*, 2025b.
- Di Jin, Eileen Pan, Nassim Oufattole, Wei-Hung Weng, Hanyi Fang, and Peter Szolovits. What disease does this patient have. *A Large-scale Open Domain Question Answering Dataset from Medical Exams. arXiv [cs. CL]*, 2020.
- Qiao Jin, Bhuwan Dhingra, Zhengping Liu, William Cohen, and Xinghua Lu. Pubmedqa: A dataset for biomedical research question answering. In *Proceedings of the 2019 conference on empirical methods in natural language processing and the 9th international joint conference on natural language processing (EMNLP-IJCNLP)*, pp. 2567–2577, 2019.
- Vladimir Karpukhin, Barlas Oguz, Sewon Min, Patrick SH Lewis, Ledell Wu, Sergey Edunov, Danqi Chen, and Wen-tau Yih. Dense passage retrieval for open-domain question answering. In *EMNLP (1)*, pp. 6769–6781, 2020.
- Tom Kwiatkowski, Jennimaria Palomaki, Olivia Redfield, Michael Collins, Ankur Parikh, Chris Alberti, Danielle Epstein, Illia Polosukhin, Jacob Devlin, Kenton Lee, et al. Natural questions: a benchmark for question answering research. *Transactions of the Association for Computational Linguistics*, 7:453–466, 2019.
- Siheng Li, Zhanhui Zhou, Wai Lam, Chao Yang, and Chaochao Lu. Repo: Replay-enhanced policy optimization. *arXiv preprint arXiv:2506.09340*, 2025a.
- Xiaoxi Li, Jiajie Jin, Yujia Zhou, Yongkang Wu, Zhonghua Li, Ye Qi, and Zhicheng Dou. Retrollm: Empowering large language models to retrieve fine-grained evidence within generation. In *Proceedings of the 63rd Annual Meeting of the Association for Computational Linguistics (Volume 1: Long Papers)*, pp. 16754–16779, 2025b.

- Xuefeng Li, Haoyang Zou, and Pengfei Liu. Torl: Scaling tool-integrated rl. *arXiv preprint arXiv:2503.23383*, 2025c.
- Xi Victoria Lin, Xilun Chen, Mingda Chen, Weijia Shi, Maria Lomeli, Richard James, Pedro Rodriguez, Jacob Kahn, Gergely Szilvasy, Mike Lewis, et al. Ra-dit: Retrieval-augmented dual instruction tuning. In *The Twelfth International Conference on Learning Representations*, 2023.
- Aixin Liu, Bei Feng, Bing Xue, Bingxuan Wang, Bochao Wu, Chengda Lu, Chenggang Zhao, Chengqi Deng, Chenyu Zhang, Chong Ruan, et al. Deepseek-v3 technical report. *arXiv preprint arXiv:2412.19437*, 2024.
- Che Liu, Haozhe Wang, Jiazhen Pan, Zhongwei Wan, Yong Dai, Fangzhen Lin, Wenjia Bai, Daniel Rueckert, and Rossella Arcucci. Beyond distillation: Pushing the limits of medical llm reasoning with minimalist rule-based rl. *arXiv preprint arXiv:2505.17952*, 2025.
- Fanbin Lu, Zhisheng Zhong, Shu Liu, Chi-Wing Fu, and Jiaya Jia. Arpo: End-to-end policy optimization for gui agents with experience replay. *arXiv preprint arXiv:2505.16282*, 2025.
- Rémi Munos, Tom Stepleton, Anna Harutyunyan, and Marc Bellemare. Safe and efficient off-policy reinforcement learning. *Advances in neural information processing systems*, 29, 2016.
- Ofir Nachum, Mohammad Norouzi, Kelvin Xu, and Dale Schuurmans. Trust-pcl: An off-policy trust region method for continuous control. *arXiv preprint arXiv:1707.01891*, 2017.
- Reiichiro Nakano, Jacob Hilton, Suchir Balaji, Jeff Wu, Long Ouyang, Christina Kim, Christopher Hesse, Shantanu Jain, Vineet Kosaraju, William Saunders, et al. Webgpt: Browser-assisted question-answering with human feedback. *arXiv preprint arXiv:2112.09332*, 2021.
- Long Ouyang, Jeffrey Wu, Xu Jiang, Diogo Almeida, Carroll Wainwright, Pamela Mishkin, Chong Zhang, Sandhini Agarwal, Katarina Slama, Alex Ray, et al. Training language models to follow instructions with human feedback. *Advances in neural information processing systems*, 35:27730–27744, 2022.
- Ankit Pal, Logesh Kumar Umapathi, and Malaikannan Sankarasubbu. Medmcqa: A large-scale multi-subject multi-choice dataset for medical domain question answering. In *Conference on health, inference, and learning*, pp. 248–260. PMLR, 2022.
- Doina Precup, Richard S Sutton, and Satinder Singh. Eligibility traces for off-policy policy evaluation. *International Conference on Machine Learning (ICML)*, pp. 759–766, 2000.
- Zehan Qi, Xiao Liu, Iat Long Iong, Hanyu Lai, Xueqiao Sun, Wenyi Zhao, Yu Yang, Xinyue Yang, Jiadai Sun, Shuntian Yao, et al. Webrl: Training llm web agents via self-evolving online curriculum reinforcement learning. *arXiv preprint arXiv:2411.02337*, 2024.
- Cheng Qian, Emre Can Acikgoz, Qi He, Hongru Wang, Xiushi Chen, Dilek Hakkani-Tür, Gokhan Tur, and Heng Ji. Toolrl: Reward is all tool learning needs. *arXiv preprint arXiv:2504.13958*, 2025.
- Rafael Rafailov, Archit Sharma, Eric Mitchell, Christopher D Manning, Stefano Ermon, and Chelsea Finn. Direct preference optimization: Your language model is secretly a reward model. *Advances in neural information processing systems*, 36:53728–53741, 2023.

- David Rein, Betty Li Hou, Asa Cooper Stickland, Jackson Petty, Richard Yuanzhe Pang, Julien Dirani, Julian Michael, and Samuel R Bowman. Gpqa: A graduate-level google-proof q&a benchmark. In *First Conference on Language Modeling*, 2024.
- Nicolas Le Roux, Marc G Bellemare, Jonathan Lebensold, Arnaud Bergeron, Joshua Greaves, Alex Fréchet, Carolyne Pelletier, Eric Thibodeau-Laufer, Sándor Toth, and Sam Work. Tapered off-policy reinforce: Stable and efficient reinforcement learning for llms. *arXiv preprint arXiv:2503.14286*, 2025.
- Timo Schick, Jane Dwivedi-Yu, Roberto Dessì, Roberta Raileanu, Maria Lomeli, Eric Hambro, Luke Zettlemoyer, Nicola Cancedda, and Thomas Scialom. Toolformer: Language models can teach themselves to use tools. *Advances in Neural Information Processing Systems*, 36:68539–68551, 2023.
- John Schulman, Filip Wolski, Prafulla Dhariwal, Alec Radford, and Oleg Klimov. Proximal policy optimization algorithms. *arXiv preprint arXiv:1707.06347*, 2017.
- Zhihong Shao, Peiyi Wang, Qihao Zhu, Runxin Xu, Junxiao Song, Xiao Bi, Haowei Zhang, Mingchuan Zhang, YK Li, Yang Wu, et al. Deepseekmath: Pushing the limits of mathematical reasoning in open language models. *arXiv preprint arXiv:2402.03300*, 2024.
- Noah Shinn, Federico Cassano, Ashwin Gopinath, Karthik Narasimhan, and Shunyu Yao. Reflexion: Language agents with verbal reinforcement learning. *Advances in Neural Information Processing Systems*, 36:8634–8652, 2023.
- Kimi Team, Yifan Bai, Yiping Bao, Guanduo Chen, Jiahao Chen, Ningxin Chen, Ruijue Chen, Yanru Chen, Yuankun Chen, Yutian Chen, et al. Kimi k2: Open agentic intelligence. *arXiv preprint arXiv:2507.20534*, 2025.
- Liang Wang, Nan Yang, Xiaolong Huang, Binxing Jiao, Linjun Yang, Daxin Jiang, Rangan Majumder, and Furu Wei. Text embeddings by weakly-supervised contrastive pre-training. *arXiv preprint arXiv:2212.03533*, 2022.
- Yubo Wang, Xueguang Ma, Ge Zhang, Yuansheng Ni, Abhranil Chandra, Shiguang Guo, Weiming Ren, Aaran Arulraj, Xuan He, Ziyang Jiang, et al. Mmlu-pro: A more robust and challenging multi-task language understanding benchmark. *Advances in Neural Information Processing Systems*, 37: 95266–95290, 2024.
- Jason Wei, Xuezhi Wang, Dale Schuurmans, Maarten Bosma, Fei Xia, Ed Chi, Quoc V Le, Denny Zhou, et al. Chain-of-thought prompting elicits reasoning in large language models. *Advances in neural information processing systems*, 35:24824–24837, 2022.
- Zhepei Wei, Wenlin Yao, Yao Liu, Weizhi Zhang, Qin Lu, Liang Qiu, Changlong Yu, Puyang Xu, Chao Zhang, Bing Yin, et al. Webagent-r1: Training web agents via end-to-end multi-turn reinforcement learning. *arXiv preprint arXiv:2505.16421*, 2025.
- Ronald J Williams. Simple statistical gradient-following algorithms for connectionist reinforcement learning. *Machine learning*, 8(3):229–256, 1992.

- Jianhao Yan, Yafu Li, Zican Hu, Zhi Wang, Ganqu Cui, Xiaoye Qu, Yu Cheng, and Yue Zhang. Learning to reason under off-policy guidance. *arXiv preprint arXiv:2504.14945*, 2025.
- Shunyu Yao, Jeffrey Zhao, Dian Yu, Nan Du, Izhak Shafran, Karthik Narasimhan, and Yuan Cao. React: Synergizing reasoning and acting in language models. In *International Conference on Learning Representations (ICLR)*, 2023.
- Qiyang Yu, Zheng Zhang, Ruofei Zhu, Yufeng Yuan, Xiaochen Zuo, Yu Yue, Weinan Dai, Tiantian Fan, Gaohong Liu, Lingjun Liu, et al. Dapo: An open-source llm reinforcement learning system at scale. *arXiv preprint arXiv:2503.14476*, 2025.
- Yufeng Yuan, Yu Yue, Ruofei Zhu, Tiantian Fan, and Lin Yan. What’s behind ppo’s collapse in long-cot? value optimization holds the secret. *arXiv preprint arXiv:2503.01491*, 2025.
- Siliang Zeng, Quan Wei, William Brown, Oana Frunza, Yuriy Nevmyvaka, and Mingyi Hong. Reinforcing multi-turn reasoning in llm agents via turn-level credit assignment. *arXiv preprint arXiv:2505.11821*, 2025.
- Chujie Zheng, Shixuan Liu, Mingze Li, Xiong-Hui Chen, Bowen Yu, Chang Gao, Kai Dang, Yuqiong Liu, Rui Men, An Yang, Jingren Zhou, and Junyang Lin. Group sequence policy optimization. *arXiv preprint arXiv:2507.18071*, 2025.
- Yifei Zhou, Andrea Zanette, Jiayi Pan, Sergey Levine, and Aviral Kumar. Archer: Training language model agents via hierarchical multi-turn rl. *arXiv preprint arXiv:2402.19446*, 2024.
- Yuxin Zuo, Shang Qu, Yifei Li, Zhangren Chen, Xuekai Zhu, Ermo Hua, Kaiyan Zhang, Ning Ding, and Bowen Zhou. Medxpertqa: Benchmarking expert-level medical reasoning and understanding. *arXiv preprint arXiv:2501.18362*, 2025.

A Appendix

A.1 Representative Failure Cases

To provide concrete evidence for the instability discussed above, we present representative failure cases from failed training runs. In the visualization, green tokens indicate samples that are clipped with importance sampling ratios smaller than $1 - \epsilon$, while red tokens correspond to clipped samples with ratios larger than $1 + \epsilon$. We observe that the majority of clipped tokens are associated with format-related symbols, such as angle brackets and other structural markers, rather than semantic content tokens. This observation suggests that token-level credit assignment is particularly prone to overestimating or underestimating frequently occurring format tokens, whose repetition amplifies the variance of importance sampling. As a consequence, the policy is driven to over-optimize these non-semantic tokens. In the 247th epoch, the resulting logical inconsistency in the generated output (e.g., “worsened by eating and improved by eating”) arises from unstable gradient updates under the token-level PPO method, where high-variance off-policy importance sampling produces unreliable gradient updates. This effect becomes evident as the generated output gradually violates the predefined formatting rules, leading to failed tool invocations. Once the format constraints are broken, downstream tool calls can no longer be executed correctly, ultimately triggering training collapse.

Generation on 243rd epoch

```
<think>
The patient is experiencing lower abdominal pain, vaginal discharge, painful
intercourse, and painful urination, which are common symptoms of a genital infection.
I'm going to <search> pelvic inflammatory disease </search> > Based on the symptoms
and the result
I'm going to <search> PID diagnosis </search> Multiple pathogens can cause
pelvic <think>
I'm going to <search> chlamydial infections </search>, there was some thought that
""Chlamydia"<think>
Based on clinical findings and symptoms <answer>E</answer>
```

Generation on 247th epoch

```
<think>
The patient is experiencing symptoms of gastroparesis, including bloating, nausea,
and dark stools, which are worsened by eating and improved by eating.
I'll <search> gastroparesis </search> assistant <think>
<search> gastroesophageal reflux disease complications </search><think>
<b <think >
assistant '),
<Bassistant <think>
assistant
```

A.2 Proof of Lemma 4.1

The proof establishes turn-level credit assignment by first reformulating the PPO objective with indicator functions, then computing how the gradient with respect to a single token depends only on its containing turn due to locality. The key insight is that the turn-level importance weight derivative yields a scaling factor of $\frac{w_k^{\text{turn}}(\theta)}{|y^k|}$, where the $\frac{1}{|y^k|}$ term arises from the geometric mean structure of the turn-level importance ratio. Finally, aggregating over all tokens via the multivariable chain rule produces the claimed gradient form where each turn receives credit proportional to $w_k^{\text{turn}}(\theta) \frac{\hat{A}^k}{|y^k|}$, combining importance weighting, accumulated advantage, and length normalization.

We now proceed with the lemma proof. We derive the gradient of the Turn-PPO objective

$\mathcal{J}_{\text{Turn-PPO}}(\theta)$ defined in Eq. 3. Beginning with the objective in expanded form:

$$\begin{aligned}
& \mathcal{J}_{\text{Turn-PPO}}(\theta) \\
&= \mathbb{E}_{x \sim \mathcal{D}, y \sim \pi_{\theta_{\text{old}}}(\cdot|x)} \left[\frac{1}{|y|} \sum_{k=1}^K \sum_{t=t_k^{\text{start}}}^{t_k^{\text{end}}} \min \left\{ w_k^{\text{turn}}(\theta) \hat{A}_t, \text{clip}(w_k^{\text{turn}}(\theta), 1 - \epsilon, 1 + \epsilon) \hat{A}_t \right\} \right] \\
&= \mathbb{E}_{x \sim \mathcal{D}, y \sim \pi_{\theta_{\text{old}}}(\cdot|x)} \left[\frac{1}{|y|} \sum_{k=1}^K \sum_{t=t_k^{\text{start}}}^{t_k^{\text{end}}} \left(\mathbb{1}_{(k,t) \in \mathcal{B}_{\text{turn}}} w_k^{\text{turn}}(\theta) \hat{A}_t + \mathbb{1}_{(k,t) \in \mathcal{B}_{\text{turn}}^c} \text{clip}(w_k^{\text{turn}}(\theta), 1 - \epsilon, 1 + \epsilon) \hat{A}_t \right) \right], \tag{16}
\end{aligned}$$

where¹ Eq. 16 follows from decomposing the min function using indicator functions. The indicator function $\mathbb{1}_{(k,t) \in \mathcal{B}_{\text{turn}}} = 1$, if the token index t within turn k belongs to the set $\mathcal{B}_{\text{turn}}$ and 0 otherwise. The set $\mathcal{B}_{\text{turn}} = \mathcal{B}_{\text{turn}}^+ \cup \mathcal{B}_{\text{turn}}^-$ represents the indices of tokens within turns where clipping is inactive. Together, the set $\mathcal{B}_{\text{turn}}$ and its complement $\mathcal{B}_{\text{turn}}^c$ partition the space of token indices across all turns, satisfying $\mathcal{B}_{\text{turn}} \cup \mathcal{B}_{\text{turn}}^c = \{1, 2, \dots, |y|\}$ and $\mathcal{B}_{\text{turn}} \cap \mathcal{B}_{\text{turn}}^c = \emptyset$. For token indices $(k, t) \in \mathcal{B}_{\text{turn}}$, the min operation selects the unclipped term $w_k^{\text{turn}}(\theta) \hat{A}_t$; otherwise, for $(k, t) \in \mathcal{B}_{\text{turn}}^c$, it selects the clipped term $\text{clip}(w_k^{\text{turn}}(\theta), 1 - \epsilon, 1 + \epsilon) \hat{A}_t$.

Taking the gradient with respect to $\log \pi_{\theta}(y_{t'}|x, y_{<t'})$ where $t' \in [t_{k'}^{\text{start}}, t_{k'}^{\text{end}}]$ (i.e., token t' belongs to turn k'), we get

$$\frac{\partial \mathcal{J}_{\text{Turn-PPO}}(\theta)}{\partial \log \pi_{\theta}(y_{t'}|x, y_{<t'})} = \mathbb{E} \left[\frac{1}{|y|} \sum_{k=1}^K \sum_{t=t_k^{\text{start}}}^{t_k^{\text{end}}} \mathbb{1}_{(k,t) \in \mathcal{B}_{\text{turn}}} \frac{\partial w_k^{\text{turn}}(\theta)}{\partial \log \pi_{\theta}(y_{t'}|x, y_{<t'})} \hat{A}_t \right] \tag{17}$$

$$= \mathbb{E} \left[\frac{1}{|y|} \sum_{t=t_{k'}^{\text{start}}}^{t_{k'}^{\text{end}}} \mathbb{1}_{(k,t) \in \mathcal{B}_{\text{turn}}} \frac{\partial w_{k'}^{\text{turn}}(\theta)}{\partial \log \pi_{\theta}(y_{t'}|x, y_{<t'})} \hat{A}_t \right], \tag{18}$$

where Eq. 17 follows since clipped terms have zero gradients by definition of the clipping function; and Eq. 18 follows since $w_k^{\text{turn}}(\theta)$ depends only on tokens within turn k . Since token t' belongs to turn k' , we have $\frac{\partial w_k^{\text{turn}}(\theta)}{\partial \log \pi_{\theta}(y_{t'}|x, y_{<t'})} = 0$ for all $k \neq k'$ due to disjoint turn boundaries.

Next, we evaluate the derivative of $w_{k'}^{\text{turn}}(\theta)$ with respect to the log probability. Recall that

¹For notational brevity, we drop the expectation subscript in what follows, with all expectations taken over the same joint distribution where $x \sim \mathcal{D}$ and $y \sim \pi_{\theta_{\text{old}}}(\cdot|x)$.

$w_{k'}^{\text{turn}}(\theta)$ is defined as

$$\begin{aligned}
w_{k'}^{\text{turn}}(\theta) &= \left(\frac{\pi_{\theta}(y^{k'}|x, y_{<k'})}{\pi_{\theta_{\text{old}}}(y^{k'}|x, y_{<k'})} \right)^{\frac{1}{|y^{k'}|}} \\
&= \left(\prod_{t=t_{k'}^{\text{start}}}^{t_{k'}^{\text{end}}} \frac{\pi_{\theta}(y_t|x, y_{<t})}{\pi_{\theta_{\text{old}}}(y_t|x, y_{<t})} \right)^{\frac{1}{|y^{k'}|}} \\
&= \exp \left(\frac{1}{|y^{k'}|} \sum_{t=t_{k'}^{\text{start}}}^{t_{k'}^{\text{end}}} [\log \pi_{\theta}(y_t|x, y_{<t}) - \log \pi_{\theta_{\text{old}}}(y_t|x, y_{<t})] \right) \\
&= \exp \left(-\frac{1}{|y^{k'}|} \sum_{t=t_{k'}^{\text{start}}}^{t_{k'}^{\text{end}}} \log \pi_{\theta_{\text{old}}}(y_t|x, y_{<t}) \right) \cdot \exp \left(\frac{1}{|y^{k'}|} \sum_{t=t_{k'}^{\text{start}}}^{t_{k'}^{\text{end}}} \log \pi_{\theta}(y_t|x, y_{<t}) \right), \quad (19)
\end{aligned}$$

where the first exponential term in Eq. 19 is constant with respect to θ . We can write $w_{k'}^{\text{turn}}(\theta) = \kappa \cdot \exp(f(\theta))$ where

$$\begin{aligned}
\kappa &= \exp \left(-\frac{1}{|y^{k'}|} \sum_{t=t_{k'}^{\text{start}}}^{t_{k'}^{\text{end}}} \log \pi_{\theta_{\text{old}}}(y_t|x, y_{<t}) \right), \\
f(\theta) &= \frac{1}{|y^{k'}|} \sum_{t=t_{k'}^{\text{start}}}^{t_{k'}^{\text{end}}} \log \pi_{\theta}(y_t|x, y_{<t}). \quad (20)
\end{aligned}$$

Consequently, the derivative of $w_{k'}^{\text{turn}}(\theta)$ with respect to the log probability is evaluated as

$$\frac{\partial w_{k'}^{\text{turn}}(\theta)}{\partial \log \pi_{\theta}(y_{t'}|x, y_{<t'})} = \kappa \cdot \exp(f(\theta)) \cdot \frac{\partial f(\theta)}{\partial \log \pi_{\theta}(y_{t'}|x, y_{<t'})} \quad (21)$$

$$\begin{aligned}
&= w_{k'}^{\text{turn}}(\theta) \cdot \frac{\partial}{\partial \log \pi_{\theta}(y_{t'}|x, y_{<t'})} \left[\frac{1}{|y^{k'}|} \sum_{t=t_{k'}^{\text{start}}}^{t_{k'}^{\text{end}}} \log \pi_{\theta}(y_t|x, y_{<t}) \right] \\
&= w_{k'}^{\text{turn}}(\theta) \cdot \frac{1}{|y^{k'}|} \cdot \frac{\partial \log \pi_{\theta}(y_{t'}|x, y_{<t'})}{\partial \log \pi_{\theta}(y_{t'}|x, y_{<t'})} \quad (22)
\end{aligned}$$

$$= w_{k'}^{\text{turn}}(\theta) \cdot \frac{1}{|y^{k'}|}, \quad (23)$$

where Eq. 21 follows from the chain rule; and Eq. 22 follows since only the term with index $t = t'$ in the summation depends on $\log \pi_{\theta}(y_{t'}|x, y_{<t'})$. Substituting Eq. 23 back into Eq. 18, we get

$$\frac{\partial \mathcal{J}_{\text{Turn-PPO}}(\theta)}{\partial \log \pi_{\theta}(y_{t'}|x, y_{<t'})} = \mathbb{E} \left[\frac{w_{k'}^{\text{turn}}(\theta)}{|y| \cdot |y^{k'}|} \sum_{t=t_{k'}^{\text{start}}}^{t_{k'}^{\text{end}}} \mathbf{1}_{(k,t) \in \mathcal{B}_{\text{turn}}} \hat{A}_t \right]. \quad (24)$$

Finally, from Eq. 16, the full gradient is given by

$$\nabla_{\theta} \mathcal{J}_{\text{Turn-PPO}}(\theta) = \sum_{k=1}^K \sum_{t=t_k^{\text{start}}}^{t_k^{\text{end}}} \frac{\partial \mathcal{J}_{\text{Turn-PPO}}(\theta)}{\partial \log \pi_{\theta}(y_t | x, y_{<t})} \nabla_{\theta} \log \pi_{\theta}(y_t | x, y_{<t}) \quad (25)$$

$$= \sum_{k=1}^K \sum_{t=t_k^{\text{start}}}^{t_k^{\text{end}}} \mathbb{E} \left[\frac{w_k^{\text{turn}}(\theta)}{|y| \cdot |y^k|} \sum_{j=t_k^{\text{start}}}^{t_k^{\text{end}}} \mathbb{1}_{(k,j) \in \mathcal{B}_{\text{turn}}} \hat{A}_j \right] \nabla_{\theta} \log \pi_{\theta}(y_t | x, y_{<t}) \quad (26)$$

$$= \mathbb{E} \left[\sum_{k=1}^K \frac{w_k^{\text{turn}}(\theta)}{|y| \cdot |y^k|} \left(\sum_{j=t_k^{\text{start}}}^{t_k^{\text{end}}} \mathbb{1}_{(k,j) \in \mathcal{B}_{\text{turn}}} \hat{A}_j \right) \sum_{t=t_k^{\text{start}}}^{t_k^{\text{end}}} \nabla_{\theta} \log \pi_{\theta}(y_t | x, y_{<t}) \right] \quad (27)$$

$$= \mathbb{E} \left[\sum_{k=1}^K \frac{w_k^{\text{turn}}(\theta)}{|y| \cdot |y^k|} \left(\sum_{j=t_k^{\text{start}}}^{t_k^{\text{end}}} \mathbb{1}_{(k,j) \in \mathcal{B}_{\text{turn}}} \hat{A}_j \right) \nabla_{\theta} \log \pi_{\theta}(y^k | x, y^{<k}) \right] \quad (28)$$

where Eq. 25 applies the multivariable chain rule; Eq. 26 follows from Eq. 24; Eq. 27 uses the chain rule identity $\nabla_{\theta} \log \pi_{\theta}(y^k | x, y^{<k}) = \sum_{t=t_k^{\text{start}}}^{t_k^{\text{end}}} \nabla_{\theta} \log \pi_{\theta}(y_t | x, y_{<t})$; and Eq. 28 follows by defining $\hat{A}^k := \sum_{j=t_k^{\text{start}}}^{t_k^{\text{end}}} \mathbb{1}_{(k,j) \in \mathcal{B}_{\text{turn}}} \hat{A}_j$. This completes the proof of Lemma 4.1. \blacksquare

A.3 Proof of Lemma 4.2

The token-level PPO objective function can be expressed as

$$\begin{aligned} \mathcal{J}_{\text{PPO}}(\theta) &= \mathbb{E}_{x \sim D, y \sim \pi_{\theta_{\text{old}}}(\cdot | x)} \left[\frac{1}{|y|} \sum_{t=1}^{|y|} \min(w_t(\theta) \hat{A}_t, \text{clip}(w_t(\theta), 1 - \epsilon, 1 + \epsilon) \hat{A}_t) \right] \\ &= \mathbb{E}_{x \sim D, y \sim \pi_{\theta_{\text{old}}}(\cdot | x)} \left[\frac{1}{|y|} \sum_{t=1}^{|y|} \left(\mathbb{1}_{t \in \mathcal{B}} \cdot w_t(\theta) \hat{A}_t + \mathbb{1}_{t \in \mathcal{B}^c} \cdot \text{clip}(w_t(\theta), 1 - \epsilon, 1 + \epsilon) \hat{A}_t \right) \right], \quad (29) \end{aligned}$$

where Eq. 29 follows from the definition of the event \mathcal{B} and

$$\text{clip}(w, 1 - \epsilon, 1 + \epsilon) = \max(\min(w, 1 + \epsilon), 1 - \epsilon) = \begin{cases} 1 - \epsilon & \text{if } w < 1 - \epsilon, \\ w & \text{if } 1 - \epsilon \leq w \leq 1 + \epsilon, \\ 1 + \epsilon & \text{if } w > 1 + \epsilon. \end{cases} \quad (30)$$

Taking the gradient with respect to θ , we obtain

$$\begin{aligned} \nabla_{\theta} \mathcal{J}_{\text{PPO}}(\theta) &= \mathbb{E} \left[\frac{1}{|y|} \sum_{t=1}^{|y|} \left(\mathbb{1}_{t \in \mathcal{B}} \cdot \nabla_{\theta} w_t(\theta) \hat{A}_t + \mathbb{1}_{t \in \mathcal{B}^c} \cdot \nabla_{\theta} \text{clip}(w_t(\theta), 1 - \epsilon, 1 + \epsilon) \hat{A}_t \right) \right] \\ &= \mathbb{E} \left[\frac{1}{|y|} \sum_{t=1}^{|y|} \mathbb{1}_{t \in \mathcal{B}} \cdot \nabla_{\theta} w_t(\theta) \hat{A}_t \right] \end{aligned} \quad (31)$$

$$= \mathbb{E} \left[\frac{1}{|y|} \sum_{t=1}^{|y|} \mathbb{1}_{t \in \mathcal{B}} w_t(\theta) \nabla_{\theta} \log \pi_{\theta}(y_t | x, y_{<t}) \hat{A}_t \right], \quad (32)$$

where Eq. 31 follows from the definition of the event B^c that yields

$$\mathbb{1}_{t \in \mathcal{B}^c} \cdot \nabla_{\theta} \text{clip}(w, 1 - \epsilon, 1 + \epsilon) \hat{A}_t = \begin{cases} \nabla_{\theta}(1 - \epsilon) \hat{A}_t = 0 & \text{if } \hat{A}_t < 0 \text{ and } w_t < 1 - \epsilon, \\ \nabla_{\theta}(1 + \epsilon) \hat{A}_t = 0 & \text{if } \hat{A}_t \geq 0 \text{ and } w_t > 1 + \epsilon; \end{cases} \quad (33)$$

and Eq. 32 readily follows from the definition of $w_t(\theta)$ that leads to

$$\nabla_{\theta} w_t(\theta) = \nabla_{\theta} \frac{\pi_{\theta}(y_t | x, y_{<t})}{\pi_{\text{old}}(y_t | x, y_{<t})} = w_t(\theta) \nabla_{\theta} \log \pi_{\theta}(y_t | x, y_{<t}). \quad (34)$$

Finally, we verify that RHS of Lemma 4.2 is equal to Eq. 32 as follows:

$$\begin{aligned} &\mathbb{E} \left[\frac{1}{|y|} \sum_{t=1}^{|y|} w_t \nabla_{\theta} \log \pi_{\theta} \hat{A}_t \right] - \mathbb{E} \left[\frac{1}{|y|} \sum_{t=1}^{|y|} \mathbb{1}_{t \in \mathcal{B}^c} w_t \nabla_{\theta} \log \pi_{\theta} \hat{A}_t \right] \\ &= \mathbb{E} \left[\frac{1}{|y|} \sum_{t=1}^{|y|} \mathbb{1}_{t \in \mathcal{B}} w_t \nabla_{\theta} \log \pi_{\theta} \hat{A}_t \right], \end{aligned} \quad (35)$$

where Eq. 35 follows from $(1 - \mathbb{1}_{t \in \mathcal{B}^c}) = \mathbb{1}_{t \in \mathcal{B}}$. This completes the proof of Lemma 4.2. \blacksquare

A.4 Implementation Details

Retrieval System. A local retriever service is deployed and accessed via an HTTP interface. For each user query, we consistently return the top three passages. The dialogue is restricted to a maximum of three interaction turns.

Training Process. All experiments are run on 8 NVIDIA H100 GPUs. We activate gradient checkpointing and train under a Fully Sharded Data Parallel (FSDP) setup with offloading enabled for parameters, gradients, and optimizers. The policy network is optimized with a learning rate of 1×10^{-6} , while the critic is trained with 1×10^{-5} . Optimization proceeds for 4 epochs, with warm-up ratios of 0.285 (policy) and 0.015 (critic). The effective batch size is 512, subdivided into mini-batches of 256 and micro-batches of 64 for policy updates and 8 for critic updates. Generalized Advantage Estimation (GAE) is employed with $\lambda = 1$ and $\gamma = 1$. Input sequences are truncated to at most 4,096 tokens, with limits of 500 tokens for responses, 2,048 tokens for the initial context, and 500 tokens for retrieved passages. We adopt turn-level importance sampling combined with clipping-trigger normalization to improve training stability. Regularization follows PPO conventions

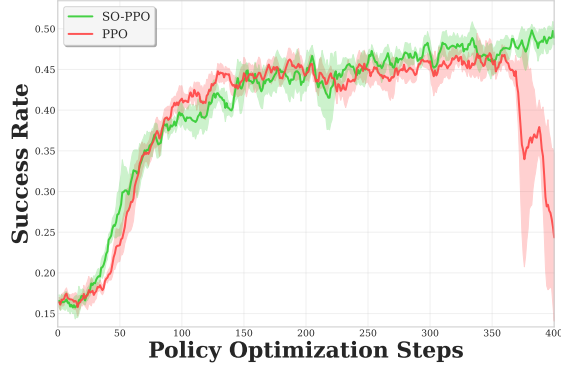


Figure 7: Experimental results of Qwen-2.5-7B policy models, with the value model also trained from Qwen-2.5-7B. Results are averaged over three trials.

with a KL coefficient of 0.001 and a clipping threshold of 0.2. Rollouts are generated using vLLM with tensor parallel size 4, GPU memory utilization set to 0.6, temperature fixed at 1.0, and top- p sampling of 1.0. The rollout and reference log-probability calculations both use a micro-batch size of 128.

Turn Boundary Identification. To implement turn-level importance sampling, we need to identify turn boundaries within the multi-turn trajectories. In our search task setup, we use the loss mask to distinguish between agent-generated content and environment responses: LLM-generated reasoning and query formulation steps are marked with 1 in the `loss_mask`, while retrieved document content is marked with 0. We define turn boundaries by grouping consecutive tokens with `loss_mask = 1` as complete turns (corresponding to the agent’s actions in our turn-level MDP), while consecutive 0s represent states (i.e., retrieved content that provides environmental feedback). These identified turn boundaries enable our algorithm to apply turn-level importance sampling and credit assignment.

A.5 Supplementary Experiments

In the following experiments, we set the training batch size to 512 and the mini-batch size to 128, which results in one on-policy update and three subsequent off-policy updates per batch. Under this more off-policy setting, our method demonstrates greater stability and more controlled performance compared to the baseline.

Figure 7 shows that, under this more off-policy regime, our method consistently exhibits greater training stability and stronger performance compared to vanilla PPO. In particular, as the degree of off-policyness increases due to repeated mini-batch reuse, the baseline method becomes increasingly unstable, whereas our approach remains robust and avoids performance collapse. These results demonstrate that the proposed method is better suited to highly off-policy training settings.

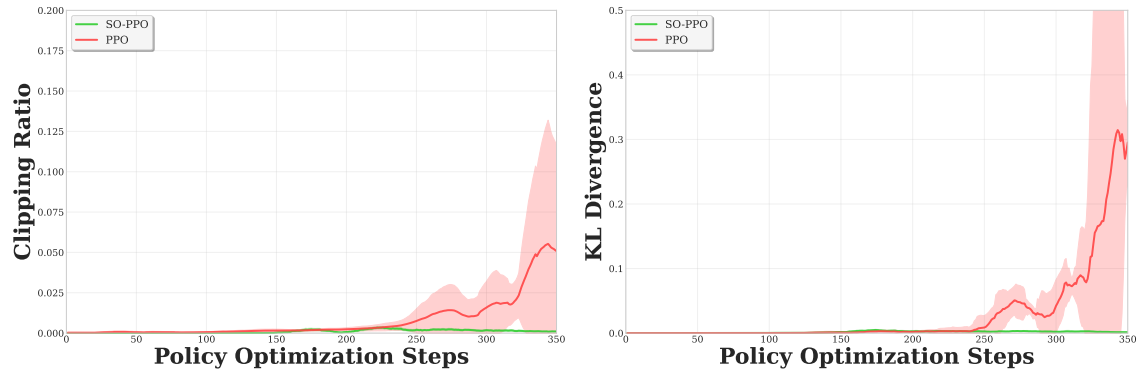


Figure 8: We report training dynamics during policy optimization on the HotpotQA dataset. **Left:** Clipping ratio. **Right:** KL divergence. SO-PPO achieve lower clipping ratios and KL divergence compared to vanilla PPO, indicating more stable training dynamics.

Prefix Prompt for the Medical Task

Answer the given medical multiple-choice question. Think step-by-step inside `<think>` and `</think>` tags.

When you encounter:

- Unfamiliar medical terminology or drug names
- Complex disease mechanisms you're uncertain about
- Specific treatment protocols or guidelines you need to verify
- Any information where you lack confidence

You can search for clarification using `<search>` query `</search>`, and results will appear between `<information>` and `</information>`. Use search strategically to fill knowledge gaps and improve answer accuracy. After sufficient reasoning and any necessary searches, provide your final answer inside `<answer>` and `</answer>` with ONLY the letter (e.g., `<answer>A</answer>`).

Table 2: A rollout example of answering a medical question.

Question: Which one of the following is not included in the treatment of malignant melanoma?

Options:

A: Radiation

B: Surgical excision

C: Chemotherapy

D: Immunotherapy

<think> Let's break down the question step by step! We're looking for the option that is not included in the treatment of malignant melanoma. </think>

<think> A: Radiation - Hmm, radiation therapy is sometimes used in combination with surgery or as palliative care for symptomatic relief. Not sure if it's the odd one out.

B: Surgical excision - Ah, surgery is a standard treatment for removing the primary tumor and any involved lymph nodes. Yes, that's a correct treatment option.

C: Chemotherapy - Chemotherapy can be used in some cases of malignant melanoma, particularly for patients with advanced disease or those who have recurrence after initial treatment. Yes, that's a valid treatment option.

D: Immunotherapy - Immunotherapy, such as pembrolizumab (Keytruda) or nivolumab (Opdivo), has shown significant efficacy in treating advanced melanoma by enhancing the body's immune response against cancer cells. Yes, that's a commonly used treatment option!

I'm getting confused about the radiation option, so let me search for clarification. </think>

<search> What is the role of radiation therapy in treating malignant melanoma? </search>

<information> Doc 1 (Melanoma): Radiation therapy is often used after surgical resection for locally or regionally advanced or unresectable metastases. It may reduce local recurrence but does not prolong survival. Doc 2 (Radiation therapy): Melanoma is generally radioresistant; radiation is mainly palliative for metastatic disease. Doc 3 (Radiation therapy): Radiation requires higher doses for melanoma than most cancers and is not curative. </information>

<think> Ah-ha! It seems that radiation therapy has a limited role in treating malignant melanoma and is mostly used in palliative care settings. It's not the first-line treatment for the disease. So, I think I can confidently say that... </think>

<answer> A </answer>
